Source Process of the Largest Aftershock (M5.5) of the 1997 Northwestern Kagoshima Earthquakes, Kyushu, Japan

Fujii, Yushiro
Faculty of Sciences, Kyushu Univeristy

Takenaka, Hiroshi
Faculty of Sciences, Kyushu University

https://doi.org/10.5109/1546836

出版情報：九州大学大学院理学研究院紀要 : Series D, Earth and planetary sciences. 31 (2), pp.59-70, 2002-02-07. Faculty of Science, Kyushu University
バージョン：
権利関係：

Mem. Fac. Sci., Kyushu Univ., Ser. D, Earth & Planet. Sci., Vol. XXXI, No. 2,
pp. 59-70, text-figs. 1-9, table 1, February 7, 2002

Source Process of the Largest Aftershock (M5.5) of the 1997 Northwestern Kagoshima Earthquakes, Kyushu, Japan

Yushiro FUJII and Hiroshi TAKENAKA

Abstract

In order to investigate the source process of the largest aftershock of the 1997 Northwestern Kagoshima earthquakes, we performed waveform modelling of the broadband strong-motion records observed at station SIBI, which include the near-field terms clearly. We found that the largest aftershock consists of at least three subevents and the initial rupture occurred at the depth of about 10km and propagated to a deeper zone. The locations and origin times of the second and third subevents were determined by a master-event method using the P-wave arrival time data of other stations as well as SIBI. The second subevent occurred at the position 1.06km to the west and 1.25km below away from the first subevent, 0.44s after the initial subevent. Also, the third subevent is located at 1.18km to the west and 1.87km below away from the first event, 0.59s after the initial subevent. The location of the third subevent is almost just under the second subevent. The focal mechanisms of the three subevents are left-lateral strike-slip and similar. Since the moment of the third subevent is by far the largest of all the subevents, the main moment release took place at the deeper part.

Keywords: the 1997 Northwestern Kagoshima earthquakes, the largest aftershock, source process, waveform modelling

I. Introduction

Two moderate earthquakes (M_{JMA}6.5, M_{JMA}6.3) occurred at the northwestern region of Kagoshima prefecture, Kyushu, Japan on March 26, 1997 and May 13, 1997 (JST; JST = UT + 9 hrs.). We distinguish these two earthquakes by calling the first mainshock and the second mainshock, respectively, because the magnitudes of the two earthquakes are very close to each other. Locations of the two mainshocks and those aftershocks are shown in Fig.1 with the focal mechanisms estimated by the Japan Meteorological Agency (JMA). Kyushu University started observing the aftershocks at Mt. Shibi (SIBI), at the center of the focal region, by a broadband strong-motion seismometer (VSE11C/12C) two days after the first mainshock occurred. During the observation period the largest aftershock (M5.5, where M indicates the local magnitude determined by the Shimabara Earthquake and Volcano Observatory (SEVO), Kyushu Univ.) occurred on April 3, 1997.

The 1997 Northwestern Kagoshima earthquakes are rare cases among inland large earthquakes, which the second mainshock occurred about one month and a half later after the first mainshock. The second mainshock has almost the same magnitude as the first mainshock and is estimated to be a multiple shock which ruptured the E-W fault and the conjugate fault (N-S).

Manuscript received September 10, 2001 ; accepted November 9, 2001.

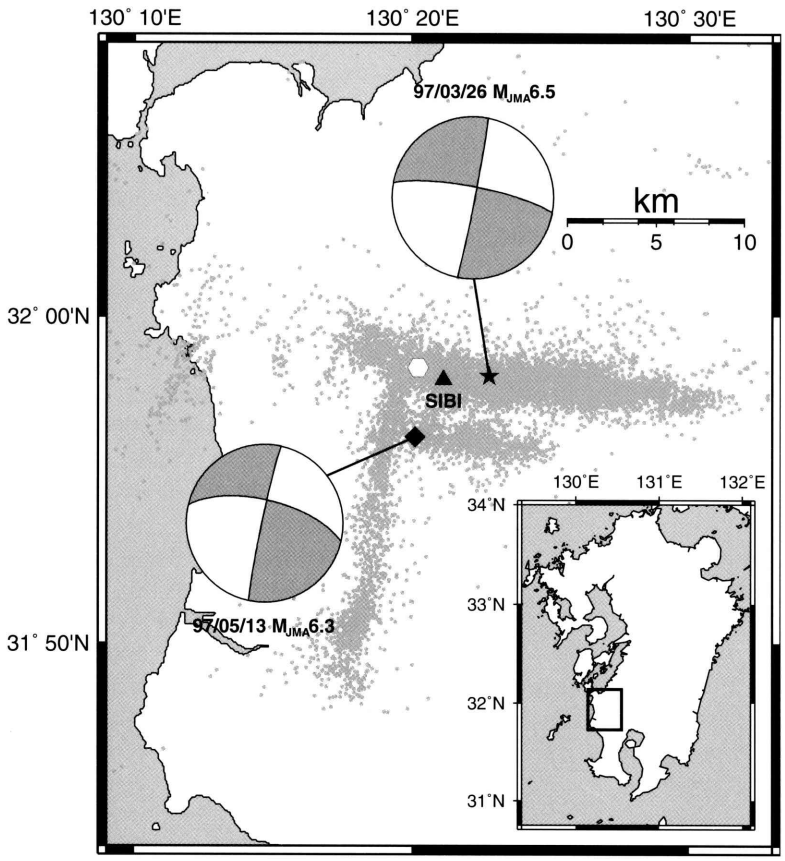

Fig.1 Epicenter distribution of the first mainshock (filled star), second mainshock (filled diamond), largest aftershock (open hexagon) and epicenters of the aftershocks occurring from 26 March 1997 to 17 September 1998 (gray dots) which are determined by the SEVO. Filled triangle indicates the station SIBI. The focal mechanisms determined by the JMA are also shown in the lower hemisphere equal-area projection. Square in the inserted map of Kyushu Island indicates the magnified area.

The purpose of this paper is to estimate the source process of the largest aftershock (M5.5) of the 1997 Northwestern Kagoshima earthquakes. This event is the largest among the aftershocks of both the first and second mainshocks, and it occurred 8 days after the first mainshock, before the second mainshock, so we are certain that the results of this study will be very significant to analyse the two mainshocks and further to investigate the tectonics of this northwestern Kagoshima region.

We perform modelling waveforms including the near-field terms to determine the source parameters (depth, strike, dip angle, rake angle, source duration, seismic moment) from the strong-motion seismograms recorded at a very hard rock site. It is very effective to use waveform data, which include the near-field terms for analysis of source processes, because the near-field terms are very long-period motion so that they are insensitive to fine underground structure. Actually, stable solutions of focal mechanisms have been determined for several earthquakes using the waveform data with the near-field terms (e.g., KANAMORI *et al.* 1990, KOSUGA 1996, TAKENAKA *et al.* 1997).

II. Waveform observation at SIBI

We analyse the waveforms of the largest aftershock recorded by a velocity-type broadband strong-motion seismometer at SIBI. The frequency characteristic of the seismometer is flat between 0.025Hz to 70Hz. SIBI is located on the granitic rock intruding into the Shimanto Supergroup, which is mainly made up of strata of sandstone and muddy stone (Editorial committee for geological map of Kagoshima Prefecture 1990). Since SIBI is a very hard rock site and is located just above the aftershock region, simple records of the aftershocks have been obtained successfully, which were little influenced by the surface geology and include the near-field terms very clearly.

Figure 2 shows the velocity record of the largest aftershock. Remarkable three *P* phases are found in the vertical component. Three *S* phases are also discriminated from each other in the two horizontal components (N-S, E-W). *S-P* times of the first, second and third phases are 1.42s, 1.55s and 1.61s, respectively. These three phases can be also detected especially for *P*-wave in the vertical components of short-period seismometers at many other stations over the northwestern part of Kyushu. These phases mean that the largest aftershock is a multiple-shock event which consists of three subevents and that locations of the subevents are different from one another.

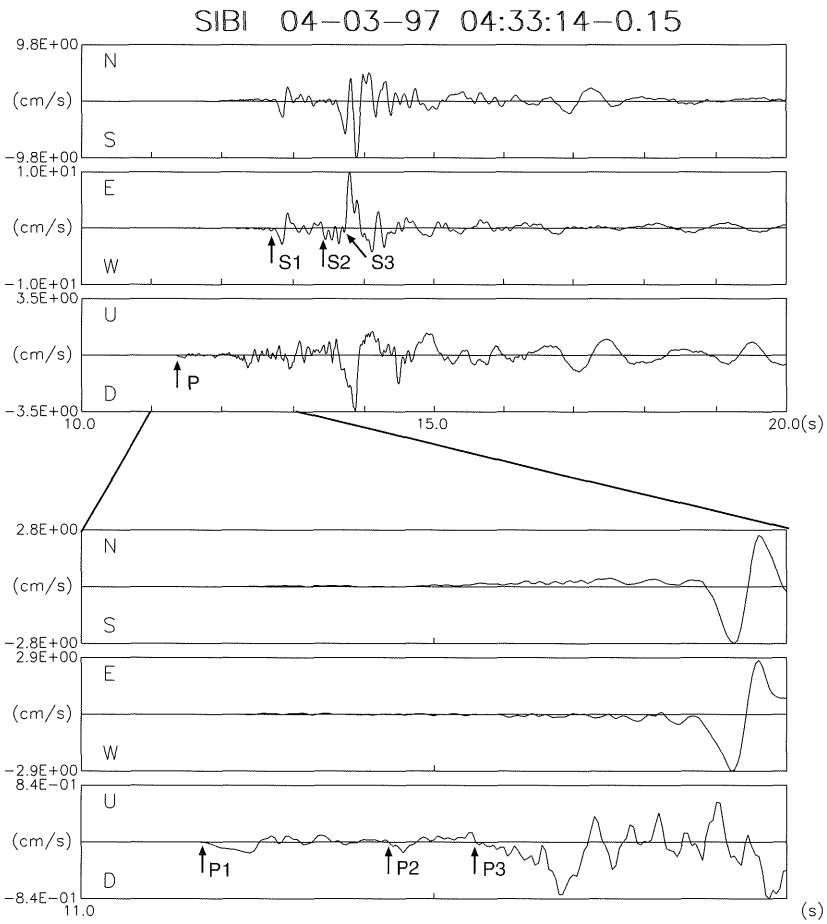

Fig.2 Velocity seismograms of the largest aftershock observed at SIBI. The arrows indicate onsets of *P* and *S* phases. Bottom figure is magnification of *P*-wave part of the top figure.

III. Locating the subevents

Seismograms of the largest aftershock have the remarkable phases especially on the part of *P*-waves. First, we estimate the locations and origin times of the second and third subevents using the arrival time data at a number of stations over the northwestern part of Kagoshima, Kyushu. For the first subevent location, we adopt the hypocenter determined by the SEVO. And we then determine the hypocenters for the second and third subevents by a master-event method which uses the time differences between the observed and computational travel times (*O-C* residuals) of a fixed master event as the station corrections.

To determine the hypocenters, we picked up the data obtained by the SEVO, NOEV (Nanseitoko Observatory for Earthquakes and Volcanos, Kagoshima Univ.), JMA, K-NET (Kyoshin Net, National Research Institute for Earth Science and Disaster Prevention (NIED), Science and Technology Agency) and FREESIA (Fundamental Research on Earthquakes and Earth's Interior Anomalies, NIED) within the northwestern part of Kagoshima in addition to the data at SIBI. The stations we selected have epicentral distances less than about 50 km and clear appearance of the second and third phases. Number of selected stations is 15 for each event and the station set used is the same for the two events. Distribution of stations used for locating the second and third subevents is shown in Fig.3. Station coverage is good for both events to determine the hypocenters. All of the data were used to only read the arrival times of the three *P* phases except SIBI's data which were employed in the waveform modelling.

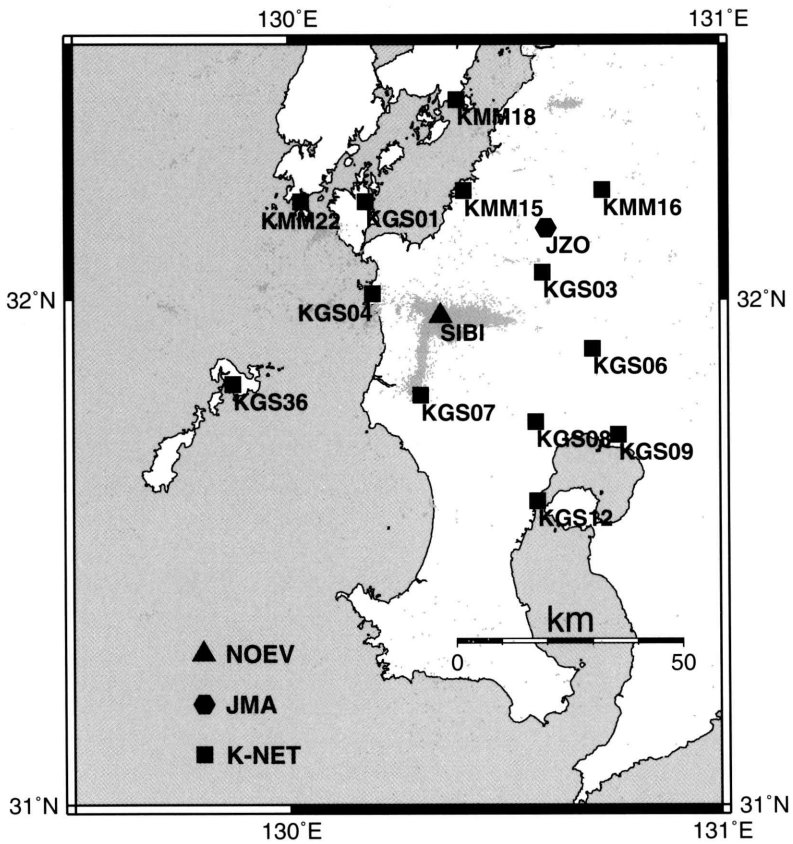

Fig.3 Locations of stations used to determine the hypocenters of the second and third subevents for the largest aftershock by the master-event method. Gray dots indicate epicenters of the earthquakes occurring from 26 March 1997 to 17 September 1998 which are determined by the SEVO.

We used the *win* system (URABE and TSUKADA 1992) to read the arrival times of the three *P* phases and the method of HIRATA and MATSU'URA (1987) to calculate the travel times and to determine the hypocenters of the second and third subevents, where we adopted the velocity structure used in the routine determinations of hypocenters by the SEVO (see Fig.4). At first, using the hypocenter of the first subevent determined by the SEVO, we then calculate the travel time of *P*-wave for all stations to obtain the *O-C* residuals of the first phase. The origin time and location of the first subevent determined by SEVO are as follows:

Origin Time: 1997/04/03 04:33:23.19 JST;

Epicenter: 31.97382 ° N ± 0.22km 130.33725 ° E ± 0.24km;

Depth: 10.10 ± 0.17km.

Next we read the arrival times of the second and third *P* phases, and then determine their hypocenters using the *O-C* residuals for the first subevent as the station corrections. In this case the first subevent has been regarded as the master event.

By using the method mentioned above we could obtain accurate locations of the second and third subevents relative to the first one.

The results are as follows: for the second subevent,

Origin Time: 1997/04/03 04:33:23.63 JST;

Epicenter: 31.97283 ° N ± 0.11km 130.32611 ° E ± 0.10km;

Depth: 11.35 ± 0.14km,

and for the third subevent,

Origin Time: 1997/04/03 04:33:23.79 JST;

Epicenter: 31.97338 ° N ± 0.12km 130.32474 ° E ± 0.10km;

Depth: 11.97 ± 0.14km.

The second subevent occurred at the position 1.06km to the west and 1.25km below away from the first subevent. Also, the third subevent is located at the place 1.18km to the west and 1.87km below away from the first subevent. The location of the third subevent is almost just under the second subevent.

Ⅳ. Waveform modelling

We obtain the displacement seismograms by integrating the velocity record at SIBI and applying a high-pass filter (higher than 0.01Hz) to remove the baseline drift. Hereafter, we call these displacement seismograms "observed seismograms".

In this study, we assume a point source for each subevent, which is located at each hypocenter determined in the previous section, to estimate source parameters, where the far-field source time function (moment rate function) is approximated by a isosceles triangle or a superposition of a few isosceles triangles. We use the reflectivity method (TAKENAKA and SASATANI 2000) to calculate Green's functions in a horizontally layered medium.

The velocity structure model used in calculation of the Green's function was assumed based on the studies of the crustal velocity structure for the south Kyushu by KAKUTA (1982), KAKUTA *et al.* (1991), and MIYAMACHI *et al.* (1998). The one-dimensional *P*-wave velocity structure of the aftershock region suggested by MIYAMACHI (1998) shows that *P*-wave velocity deeper than the depth of 4km is almost constant (about 5.9km/s). This part deeper than the depth of 4km is considered to be the basement of granite, which makes up Mt. Shibi. We put four layers on the basement layer (half-space) so that velocities of the structure model does not have strong velocity contrast but become gradually slower to the surface in the shallow area above the basement. The velocity structure model we employed is shown in Fig.4, where the ratio of *P*-wave velocity to *S*-wave velocity (V_P/V_S ratio) has been fixed to be 1.73.

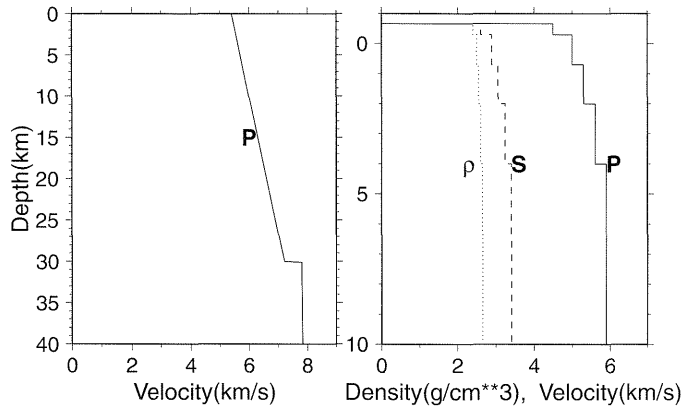

Fig.4 Left: *P*-wave velocity structure model employed to determine the hypocenters of the second and third subevents. This model has been used in the routine determinations of hypocenters by the SEVO. Right: Velocity and density structure model employed to calculate the Green's functions for SIBI. This model is based on KAKUTA (1982), KAKUTA *et al.* (1991), and MIYAMACHI *et al.* (1998).

Procedure of the waveform modelling for the largest aftershock is as follows: At first, we consider one of the three subevents. We estimate the source duration (length of the base of triangle) from *P*- and *S*-wave pulse length. Synthetic seismograms are then calculated to be compared with the observed seismograms to estimate the other source parameters (strike, dip, rake angle, and seismic moment) by trial and error. The synthetic seismograms have been high-pass filtered in the same way as the observed seismograms. No instrumental correction for the seismometer has been made because the frequency response of the seismometer is almost flat over the frequency range where the observed seismograms have most of the energy. The chain of the above steps of the procedures is applied to all subevents of the largest aftershock. We then synthesize the three synthetic seismograms corresponding to the three subevents to obtain the

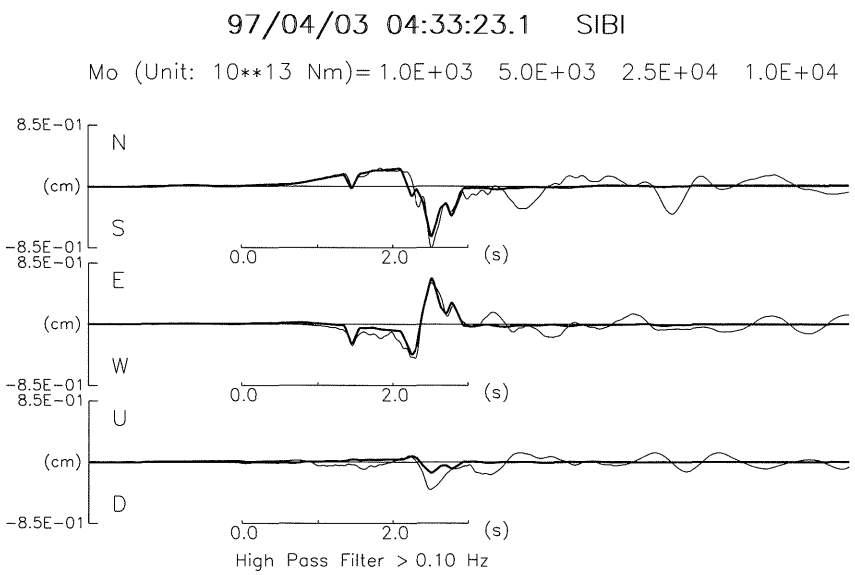

Fig.5 Comparison between the synthetic (thick line) seismograms and observed ones (thin line) obtained by integration of the velocity records for the largest aftershock, which have been all high-pass filtered (>0.1Hz) to exclude long period component. The origin time of event and the estimated seismic moment (M_0) are also shown on the top.

total synthetic seismograms for each component. In case that the fitness between synthetic and observed seismograms is not good, we reexamine the synthetic seismograms of each subevent.

On matching the synthetics with the observed seismograms, we paid attention to the near-field terms (in the strict sense, near-field and intermediate terms) which are seen as ramps between direct *P*- and *S*-waves. The reason is because the near-field terms are insensitive to fine subsurface velocity structures and extremely helpful to estimate stable solutions of the source parameters.

Figure 5 shows the total synthetic seismograms matched with the observed seismograms. The amplitudes and polarities of the synthetic seismograms fairly agree well with those of the observed ones for *P*- and *S*-wave for the horizontal components. Although the *S*-wave amplitude in the vertical component of synthetics and the observed seismograms have still a little discrepancy and the near-field terms for EW and UD components of the observed seismograms may not be fully simulated, the overall agreement between the synthetic and observed seismograms are quite well.

Moment rate function estimated is shown in Fig.6. Figure 7 shows the focal mechanisms corresponding to the first, second and third subevents with polarities of the *P*-wave motions at stations whose records are used to locate the hypocenters. The focal mechanisms estimated by the waveform modelling are left-lateral strike-slip and consistent with the distributions of the *P*-wave polarities, which indicates that obtained source parameters are reasonable. The determined source parameters for the largest aftershock are summarized in Table 1, where we have employed the definition of AKI and RICHARDS (1980) for the angle parameters. We have used four triangles totally for the source time function. The first (I) and second (II) subevents consist of only one triangle respectively, while the third subevent (III) consists of two triangles (III-1, III-2). The main reason to use two triangles is that if the moment release took place from just only the one patch (III-1), the amplitude of synthetics for the near-field terms is to be underestimated. Since the moment magnitude of the third subevent is equal to the local magnitude determined by the SEVO, it is found that the third subevent is the main event of this earthquake.

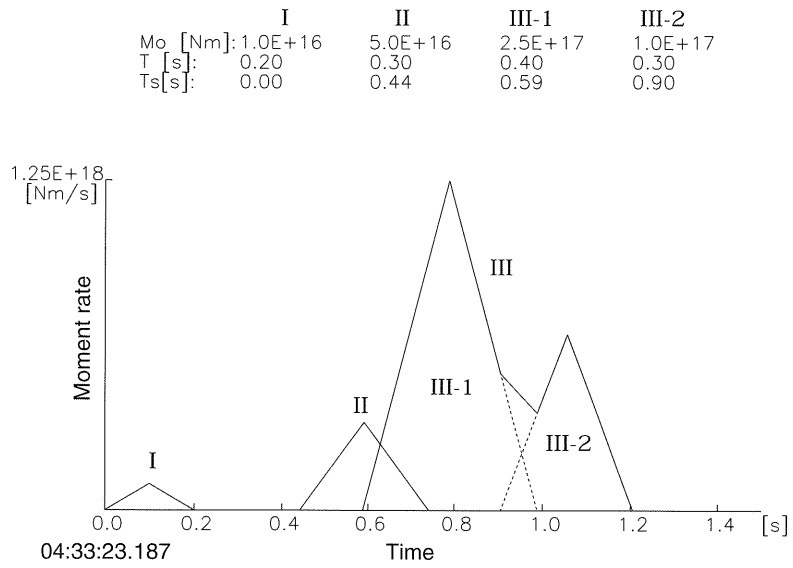

Fig.6 Moment rate function estimated for the largest aftershock. Symbols of M_0, T and T_s stand for seismic moment, source duration and time difference between the first pulse and later pulses, respectively.

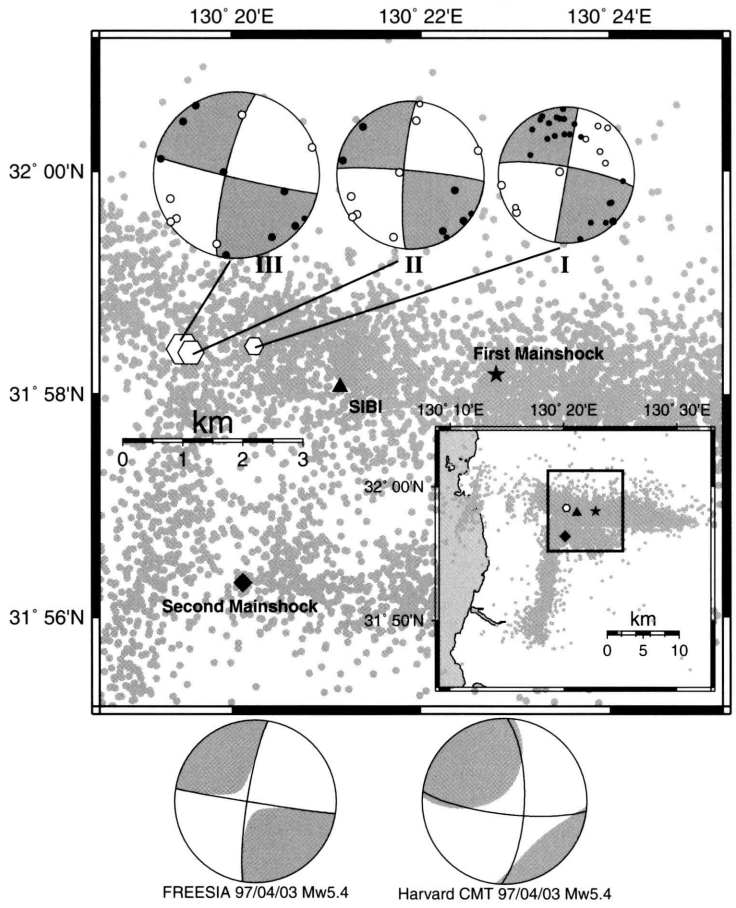

Fig.7 Estimated focal mechanism of each subevent of the largest aftershock. Polarities of *P*-wave motions corresponding to each subevent are plotted on the focal mechanism solutions by filled (up) and open (down) circles. Two focal mechanism solutions shown on the bottom are centroid moment tensor solutions determined by NIED (FREESIA) and Harvard Univ.

Table 1 Estimated source parameters for the largest aftershock

Subevent	Duration (s)	M_0 (Nm)	M_w	M	strike	dip	rake (deg)	d (km)	S (km^2)	a (km)
I	0.2	1.0×10^{16}	4.6		280	80	0	10.10	2.82	0.95
II	0.3	5.0×10^{16}	5.1		275	85	8	11.35	8.24	1.62
III	0.6	3.5×10^{17}	5.6		283	93	10.5	11.97	30.16	3.10
III-1	0.4	2.5×10^{17}	5.5						24.10	2.77
III-2	0.3	1.0×10^{17}	5.3						13.08	2.04
total		4.1×10^{17}	5.7	5.5					33.51	3.27

M_w: Moment magnitude
M : Magnitude determined by the SEVO
d : Source depth measured from the sea level
S : Area of fault estimated from (log S=M_w-4.15; WYSS, 1979)
a : Radius of the fault assumed to be a circular fault (a=$\sqrt{S/\pi}$)

V. Discussion

In order to check the stability of the focal mechanisms obtained in the previous section, we calculate the synthetic seismograms, setting the depths of the second and third subevents to be 0.14km (error range) of the hypocenters deeper than ones shown in Table 1. Figure 8 shows the synthetics with the observed seismograms. We can see no meaningful difference compared to Fig.5. This means that stable focal mechanism solutions for the subevents have been obtained within the error ranges of the locations.

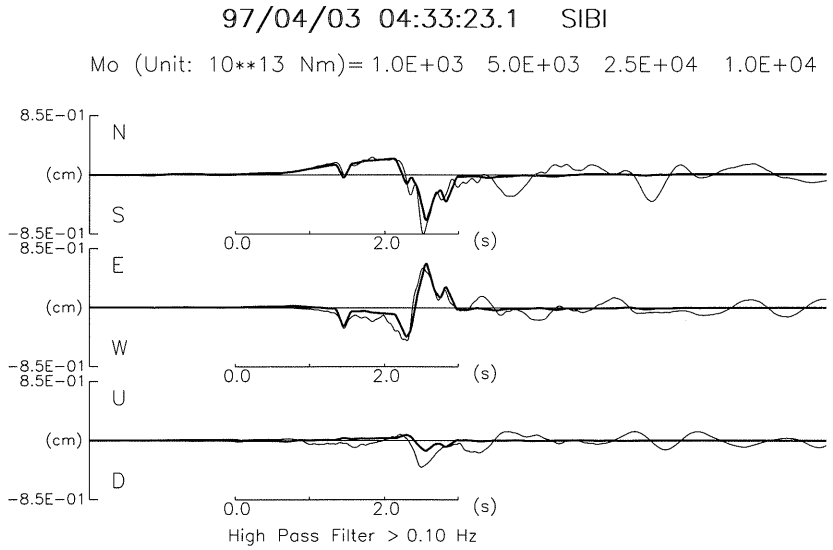

Fig.8 Comparison between the synthetic (thick line) seismograms and observed ones (thin line). Notations are the same as Fig.5. But for the synthetic seismograms, the depths of the second and third subevents are assumed to be about 0.14km (error range) deeper than ones shown in Table 1. Notice that agreement of synthetics with observed seismograms are not so spoiled comparing with Fig.5.

Focal mechanisms estimated for the largest aftershock by automated moment tensor determination conducted under FREESIA Project, NIED (FUKUYAMA *et al.*, 1998, http://argent.geo.bosai.go.jp/freesia/) and Harvard CMT solution (DZIEWONSKI *et al.*, 1999; http://www.seismology.harvard.edu) are shown at the bottom of Fig.7. The NIED solution is more similar to the focal mechanism of the three subevents we obtained than the Harvard one. Note that the focal solution estimated by the NIED is almost identical with that of the third subevent which has the largest moment release of all subevents.

Comparing the seismic moment of the three subevents, we can consider that the first subevent and the third subevent are an initial rupture and major event, respectively. There are some M 5-class events which consist of the initial rupture and main rupture subevents (multiple-shock event). One is the 1990 Odawara earthquake (M5.1). ISHIDA and KIKUCHI (1992) found that the focal mechanism inferred from the P-wave first motion is meaningfully different from that estimated from the major part of the initial portion of the broad-band waveform data. They actually obtained the better fitness between the observed and synthetic seismograms using the focal mechanism obtained from the major part of the waveforms, as comparison with those calculated for the focal mechanism deduced from the P-wave first motion. These mechanisms are strike-slip type and dip-slip type

respectively, and are significantly different from each other unlike the event studied in this paper.

The 15 October 23:19 aftershock (M_L=5.0) of the 1997 Imperial Valley earthquake is another example of M 5-class multiple-shock earthquake which has strike-slip type subevents as well as the event analysed in this study. LIU and HELMBERGER (1985) investigated the source mechanism by a waveform inversion using two horizontal components recorded at just above the source region. According to their results, the aftershock consists of two subevents which have different mechanisms each other and the second event (major event) has a seismic moment twice that of the first event.

In case of the event studied in this paper, the estimated focal mechanisms of the three subevents are very similar but not identical each other. Differences of the estimated faults parameters between the first and third subevents more than ten degree in all of strike, dip and rake (see Table 1), while those of the second subevent from the first and third subevents are less than ten degrees. In the forward modelling process of waveform at SIBI and P-wave polarity distribution, we found that change of the fault parameters more than ten degrees leads to significant variation of the fitness between the observed and computed data. Therefore we can at least say that our results suggest a slight change of the focal mechanism during the source process from the initial rupture to the main rupture.

Another noticeable source property for the largest aftershock studied here is, as we can see in Fig.9, that the rupture propagated downward and the largest moment was released at the deeper zone. MIYAMACHI *et al.* (1999) suggested from the aftershock distributions that the first mainshock ruptured the deep middle part of the low aftershock activity zone which extends from the hypocenter mainly to the western shallow area. MIYAKE *et al.* (1999) also found that a large moment of the first mainshock release took place mainly at the western part of the hypocenter with a forward modelling of strong motion records. HORIKAWA (2001) also constructed the fault model from strong motion data by an inversion method, which has a single asperity at western part from the hypocenter. In Fig.9, the asperity found by HORIKAWA (2001) is corresponding to the inactive area of the aftershocks, which is on the west of the hypocenter of the first mainshock. The first subevent of the largest aftershock is located just below that asperity, and the third subevent is located at the extreme bottom of the aftershock region. From this configuration of the asperity of the first mainshock and the subevents of the largest aftershock, we speculate that the rupture front of the first mainshock had stopped above the initial rupture point (the first subevent) of the largest aftershock, so that it had not reached to the bottom of seismogenic layer in the crust of this region.

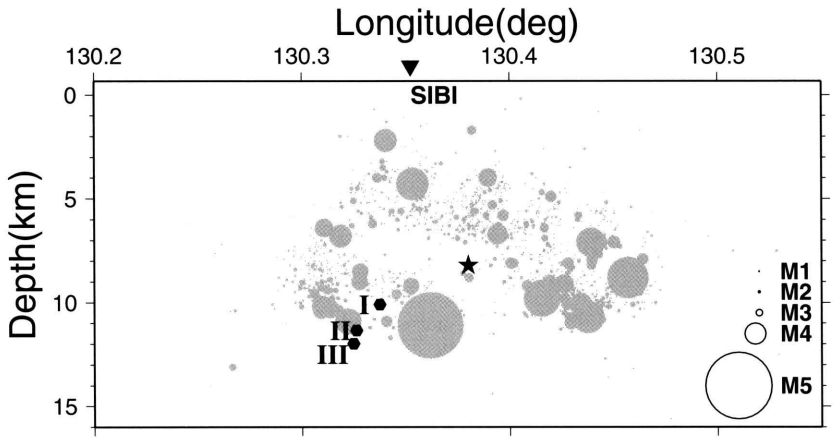

Fig.9 Vertical cross section of the aftershock distribution along the latitude. Aftershocks which occurred between the first mainshock and the largest aftershock are shown. Filled star indicates hypocenter of the first mainshock. Sizes of circles for the aftershocks (gray circle) are in proportional to the magnitude.

VI. Conclusions

We have investigated the source process of the largest aftershock for the 1997 Northwestern Kagoshima earthquakes to find this event is a multiple shock composed of at least three subevents. We first located the hypocenters of the subevents by a master-event method, and found that the largest aftershock occurred at the depth of about 10km and the rupture propagated to the deeper zone. Next we estimated the focal mechanism of each subevent through the waveform modelling.

The focal mechanisms of the three subevents are left-lateral strike-slip and similar each other. Our results suggest that the major moment of the largest aftershock was released at the deeper zone 0.59s after the initial rupture.

Acknowledgments

We used precious data recorded by NOEV, JMA, K-NET, and FREESIA. We quoted the result of "Earthquake mechanism analysis using broadband seismic waveforms conducted under FREESIA Project, NIED". The authors would like to express our gratitude to Dr. T. MATSUSHIMA (SEVO) and Dr. K. UMAKOSHI (SEVO; present: Nagasaki Univ.) for the observation at SIBI and the management of the data. SIBI is originally a permanent station of the NOEV's seismic network. Mr. K. UEHIRA (SEVO) guided us how to use the *win*-system on a master-event method. We also wish to thank Prof. S. SUZUKI for his encouragement for this study.

References

AKI, K. and RICHARDS, P. G. (1980) *Quantitative Seismology, Theory and Methods, vol.1*, W.H. Freeman, San Francisco, 557pp..

DZIEWONSKI, A. M., EKSTRÖM G. and MATERNOVSKAYA N. N. (1999) Centroid-moment tensor solutions for April-June, 1997. *Phys. Earth Planet. Int.*, **112**, 1-9.

Editorial committee for geological map of Kagoshima Prefecture (1990) *Geology of Kagoshima Prefecture*, 117pp. (in Japanese).

FUKUYAMA, E., ISHIDA, M., DREGER, D. S., and KAWAI, H. (1998) Automated seismic moment tensor determination by using on-line broadband seismic waveforms. *Zisin (J. Seis. Soc. Japan), Ser. II*, **51**, (1), 149-156 (in Japanese with English abstract).

HIRATA, H. and MATSU'URA, M. (1987) Maximum-likelihood estimation of hypocenter with origin time eliminated using nonlinear inversion technique. *Phys. Earth Planet. Inter.*, **47**, 50-60.

HORIKAWA, H. (2001) Earthquake Doublet in Kagoshima, Japan: Rupture of Asperities in a Stress Shadow. *Bull., Seism. Soc. Am.*, **91**, (1), 112-127.

ISHIDA, M. and KIKUCHI, M. (1992) A possible foreshock of a future large earthquake near Odawara, center Japan. *Geophys. Res. Lett.*, **19**, (16), 1695-1698.

KAKUTA, T. (1982) Upper crustal structure in South Kyushu. *J. Phys. Earth*, **30**, 113-129.

————, MIYAMACHI, H. and TAKAGI, A. (1991): Intermediate Earthquakes in a Northern Part of the Kyushu-Ryukyu Arc. *Zisin (J. Seis. Soc. Japan), Ser. II*, **44**, 63-74 (in Japanese with English abstract).

KANAMORI, H., MORI, J. and HEATON, T. H. (1990) The 3 December 1988, Pasadena Earthquake (M_L=4.9) recorded with the very broadband system in Pasadena. *Bull. Seism. Soc. Am.*, **80**, (2), 483-487.

KOSUGA, M. (1996) Near-field moment tensor inversion and stress field in northeastern Japan, *Ph. D. thesis, Tohoku Univ.*, 233pp..

LIU, H. and HELMBERGER, D. V. (1985) The 23:19 aftershock of the 15 October 1979 Imperial valley Earthquake: More evidence for an asperity. *Bull., Seism. Soc. Am.,* **75**, (3), 689-708.

MIYAKE, H., IWATA, T. and IRIKURA, K. (1999) Strong ground motion simulation and source modeling of the Kagoshima-ken Hokuseibu Earthquake of March 26 (M_{JMA}6.5) and May 13 (M_{JMA}6.3), 1997, using empirical Green's function method. *Zisin (J. Seis. Soc. Japan), Ser. II,* **51**, (4), 431-442 (in Japanese with English abstract).

MIYAMACHI, H., IWAKIRI, K., TSUNO, T., SHIMIZU, C., FUKUMITSU, S., KANEKO, K., SEKITANI, H., KAKUTA, T., GOTO, K., YAKIWARA, H., HIRANO, S., MATSUSHIMA, T., and SHIMIZU, H. (1998) Temporary Seismic Observation of Aftershocks for the 1997 Northwestern Earthquakes in Kagoshima Prefecture. *Geophys. Bull. Hokkaido Univ.,* **61**, 85-98 (in Japanese with English abstract).

————, ————, Yakiwara, H., Goto, K., Kakuta, T. (1999) Fine structure of aftershock distribution of the 1997 Northwestern Earthquakes with a three-dimensional velocity model. *Earth Planets Space,* **51**, 233-246.

TAKENAKA, H. and SASATANI, T. (2000) Seismic Waves in a horizontally layered half-space with a general point source. *Mem. Fac. Sci. kyushu Univ., Ser. D, Earth Planet. Sci.,* **31**, (1), 19-28.

————, FUJII, Y., OKUMURA, T. and SUZUKI S. (1997) Modelling of strong motion at Kikai Island due to aftershocks of the 1995 Amami-Oshima-Kinkai earthquakes. *J. Geography,* **106**, (4), 525-536 (in Japanese with English abstract).

URABE, T. and TSUKADA, S. (1992) *win*-A Workstation Program for Processing Waveform Data from Microearthquake Networks, *Programme Abst., Seismol. Soc. Jpn., No.2*, 331 (in Japanese).

WYSS, M. (1979) Estimating maximum expectable magnitude of earthquakes from fault dimensions. *Geology,* 7, 336-340.